A&A 377, 707–720 (2001)
DOI: 10.1051/0004-6361:20011136

Astronomy & Astrophysics

Crystalline silicon nanoparticles as carriers for the Extended Red Emission

G. Ledoux[1,2], O. Guillois[1], F. Huisken[2], B. Kohn[2], D. Porterat[1], and C. Reynaud[1]

[1] CEA/DSM/DRECAM/SPAM, CE Saclay, 91191 Gif-sur-Yvette Cedex, France
[2] Max-Planck-Institut für Strömungsforschung, Bunsenstrasse 10, 37073 Göttingen, Germany

Received 25 January 2001 / Accepted 26 July 2001

Abstract. In an attempt to determine the carrier of the Extended Red Emission (ERE), we have investigated a series of amorphous and crystalline materials: natural coal, amorphous hydrogenated carbon, amorphous hydrogenated silicon carbide, porous silicon, and crystalline silicon nanoparticles. The photoluminescence (PL) behavior of various samples of these materials upon excitation with UV light was studied at room temperature focusing on both the wavelength dependence of the photoluminescence and the PL yield. For some samples the yield is by far too low, other samples do not comply with the characteristic wavelength range of ERE. Only the samples of nanocrystalline silicon (porous silicon and silicon nanoparticles) reveal PL properties that are compatible with the astronomical observations. Besides this experimental evidence, we will supply additional arguments leading to the conclusion that silicon nanoparticles should be seriously considered as an attractive carrier for the Extended Red Emission.

Key words. interstellar medium: dust, extinction – ISM: reflection nebulae

1. Introduction

The Extended Red Emission (ERE) was first detected by Cohen et al. in 1975 in the Red Rectangle, but it was really identified as a general spectroscopic feature in 1980 by Schmidt et al. in the same object. It has now been detected in many kinds of objects such as reflection nebulae (Witt et al. 1984), planetary nebulae (Furton & Witt 1990), HII regions (Perrin & Sivan 1992), halos of galaxies (Perrin et al. 1995), and more recently even in the Diffuse Interstellar Medium (DISM) (Gordon et al. 1998). The latter observation shows that ERE is a general phenomenon. Therefore, the identification of its carrier deserves even more attention. All spectroscopic properties observed so far point to a luminescence phenomenon, most probably photoluminescence (PL), originating from some interstellar dust component. However, the real nature of the carrier is still under debate.

Recently, nanocrystalline silicon (nc-Si) has been proposed as the material responsible for ERE (Ledoux et al. 1998; Witt et al. 1998). This proposal marks a radical change in the interpretation of ERE since, until that time, it was rather associated with carbonaceous compounds such as polycyclic aromatic hydrocarbons (PAHs) (d'Hendecourt et al. 1986), hydrogenated amorphous carbons (HACs) (Duley 1985; Wdowiak et al. 1989) or quenched carbonaceous compounds (QCCs) (Sakata et al. 1992). Moreover, it was the first time that nc-Si was proposed to be a component of the interstellar dust. In order to establish nc-Si as carrier for ERE, it is necessary to explain why it is the only material exhibiting the required PL properties and to show that this proposal is compatible with the astronomical constraints.

A good overview of the characteristic properties of ERE may be found in the article by Witt et al. (1998). In what follows, we give a short summary of the most relevant observations, including some newer results:
(1) ERE always appears as a broad structureless emission band. The position of the maximum of the band varies from environment to environment and even within a given object from 600 to 850 nm. Efforts dedicated to finding luminescence between 400 and 500 nm resulted in strict upper limits consistent with the absence of photoluminescence in this spectral region (Rush & Witt 1975);
(2) The full width at half maximum (*FWHM*) of the ERE bands changes from 120 to 210 nm. This corresponds to a range from 60 to 120 nm if we consider the width in which half of the total PL energy is concentrated. In general, the bandwidth increases when the ERE becomes redder (Witt & Boroson 1990; Darbon et al. 1999a);
(3) With increasing energy and intensity of the illuminating radiation field, the maximum position of the ERE band moves to longer wavelengths (Witt et al. 1998; Darbon et al. 1999b). In addition, the conversion efficiency

Send offprint requests to: G. Ledoux,
e-mail: gledoux@gwdg.de

seems to decrease with the strength of the radiation field (Smith et al. 1999);

(4) In the DISM, the number of photons detected in the ERE band corresponds to 10% of the UV photons (from 91 to 550 nm) absorbed by the interstellar dust particles (Gordon et al. 1998). Since the measured PL intensity is determined by a product of two quantities, namely the percentage of UV photons absorbed by the particles giving rise to ERE and the PL yield (η), each of the quantities must be larger than the measured relative number of ERE photons. In particular, the yield must be larger than 0.1;

(5) In 1985, Witt and Schild found a correlation between the absorption of mid-UV photons (180−250 nm) and the ERE process. Later, in an extended analysis of various objects, Darbon et al. (1999a) pointed out that ERE has never been observed near stars whose color temperature is lower than 7000 K. These observations suggest that visible photons are not efficient in inducing ERE;

(6) From observations on planetary nebulae it is known that only carbon-rich planetary nebulae exhibit ERE (Furton & Witt 1992). However, this argument may be somewhat questionable since more recent observations, made by the Infrared Space Observatory (ISO) for example in the Red Rectangle, suggest that the distinction between carbon-rich and oxygen-rich regions is not so clear (Waters et al. 1998). It would be interesting to correlate spatially extended red emission with the C- or O-rich character in such nebulae;

(7) There is no correlation between ERE and other major spectral bands observed so far. For example, no correlation was found between ERE and the unidentified infrared bands (UIBs) (Perrin & Sivan 1992; Darbon et al. 1999b; Kerr et al. 1999). As the observations in the red rectangle have shown, there is also no correlation with the appearance of sharp red emission features (Schmidt et al. 1980; Witt & Boroson 1990; Rouan et al. 1995) nor with the 2175 Å bump in the extinction curve (Witt 1999);

(8) In contrast, ERE seems to be correlated with the thermal emission from dust between 10.5 and 12 μm (Darbon et al. 1999b).

The most severe restrictions for the ERE carriers are imposed by both the very high photoconversion efficiency and the specific spectral characteristics of the phenomenon. Carbonaceous compounds, that were originally proposed on the basis of observation (6), encounter great difficulties in fulfilling the two requirements. After a detailed examination of the PL properties of hydrogenated amorphous carbon, Witt et al. (1996) were led to the conclusion that amorphous ternary alloys such as a-$Si_{1-x}C_x$:H could be a better candidate. Considering silicon-based materials, the well-documented properties of porous silicon (Feng & Tsu 1994; Cullis et al. 1997) and the more recent results on silicon nanoparticles (Ledoux et al. 2000a) make nc-Si an attractive carrier candidate. In addition, it is interesting to note that, besides carbon, silicon is one of the most abundant elements in the interstellar dust.

In the present study, we have investigated the PL properties of a few of the solid state materials being proposed as carriers for ERE. These include samples of natural coal, amorphous hydrogenated carbon (a-C:H), amorphous hydrogenated silicon carbide (a-SiC:H), porous silicon (p-Si), and nanocrystalline silicon (nc-Si). The latter studies were carried out for an extended set of size-selected samples with mean diameters between 2 and 5 nm. Not only have we measured the spectral properties of the PL, but we have also determined the PL yields, using in all cases the same apparatus so that the results can be readily compared. From the various materials studied, we found only nanocrystalline silicon (including porous Si) to satisfy the conditions imposed by the astrophysical observations. Analysis of the PL of silicon nanoparticles in terms of the quantum confinement effect allows us to model all ERE observations reported so far and to propose a consistent interpretation of the ERE phenomenon.

The paper is organized as follows. In Sect. 2, we give a short overview of the phenomenon of photoluminescence as far as it concerns the interpretation and discussion of the present laboratory and astrophysical observations. The experimental setup will be described in Sect. 3, while the experimental results are presented in Sect. 4. There follows a comparison of the experimental data with the astronomical observations (Sect. 5), and in the discussion (Sect. 6) we will show that nc-Si represents the most promising candidate as carrier for the Extended Red Emission. Finally we will also discuss the implications of the present results on the general properties of the cosmic dust.

2. Overview of the PL process and implications for ERE

At first we will briefly discuss the mechanism of photoluminescence in semiconductors as far as it is necessary for understanding the experimental results in context with the astrophysical issue. The general mechanism of PL in solids is described in Fig. 1. When a photon of energy higher than the so-called band gap of the material (the separation between valence and conduction bands) is absorbed, an electron-hole pair is created. On a very short timescale the energy is thermalized so that the energy separation between the electron and the hole becomes approximately equal to the energy of the gap. Then the pair can radiatively recombine, giving rise to the emission of a photon (luminescence). As a result, the peak position of the photoluminescence roughly reflects the band gap of the material. In general, the yield of PL is governed by a competition between radiative and non-radiative recombination. The sources of non-radiative recombination are defects in the material (for example impurities and disorder sites in a crystal or dangling bonds on the surface). Therefore, the defects are said to quench the photoluminescence.

In metals there is no PL because there is no gap. For semiconductors, we have to distinguish between

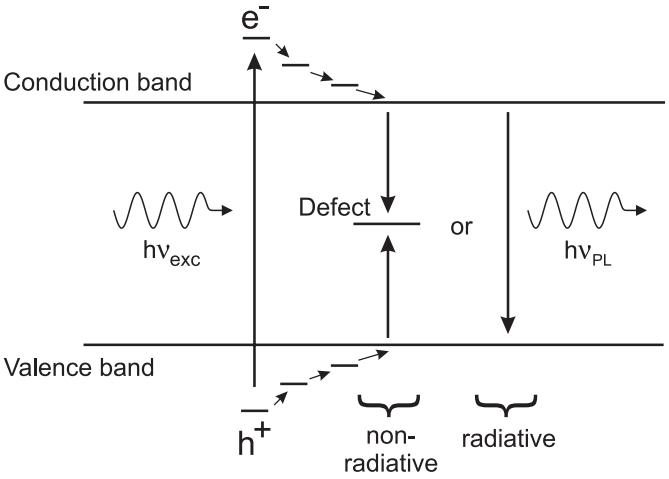

Fig. 1. PL mechanism in semiconductors: an incoming photon of sufficiently high energy $h\nu_{\mathrm{exc}}$ is absorbed by the material creating an electron-hole pair (h^+e^-). These carriers quickly thermalize to the limits of the conduction and valence bands. They can recombine either non-radiatively on defects or radiatively by emitting a PL photon with an energy close to that of the band gap.

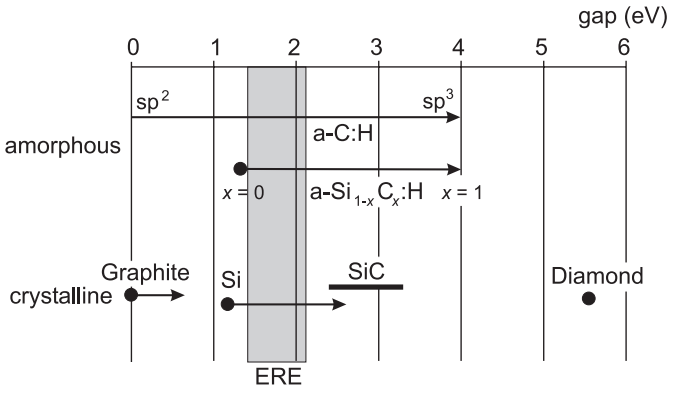

Fig. 2. Reported band gaps of different amorphous and crystalline materials containing carbon and/or silicon. The shaded area corresponds to the range of energies where ERE is observed (maximum band positions).

direct- and indirect-gap materials. For indirect-gap materials, like silicon, the radiative recombination is only possible with the assistance of momentum-conserving phonons or impurities and, therefore, the probability for the creation of PL photons is very low. Yet while this is true for bulk silicon, *nanosized* silicon particles with diameters smaller than ∼8 nm show drastically enhanced transition probability because the spatial confinement is associated with a broadening of the pair state in momentum space.

When the size is reduced to the nanometer scale the probability of non-radiative recombination decreases more and more (if we assume that the density of defects remains constant). This is because the probability for the carriers to find a defect in the core is getting smaller. On the other hand, the number of surface atoms relative to the number of volume atoms increases with decreasing size. As a result, the problem of dangling bonds becomes more pronounced for nanoparticles. Since the dangling bonds represent traps for the carriers, the surfaces of nanoparticles must be completely passivated to avoid quenching the photoluminescence. For silicon nanoparticles, this can be achieved, for example, by hydrogenation, resulting in SiH groups at the surface, or by oxidation (Wehrspohn et al. 1999; Vial et al. 1992). In any case, it should be stressed here that non-passivated silicon nanoparticles will not exhibit PL.

Another consequence of the spatial confinement of the electronic wave function in nanosized systems is the progressive widening of the band gap as the particle size is reduced. Theoretical studies have shown (Delerue et al. 1993) that, e.g. for silicon nanoparticles, the band gap increases from 1.4 to 2.5 eV when the diameter is reduced from 7 to 2 nm. As a result, the peak photoluminescence of these particles is expected to vary from 900 to 500 nm, respectively. Thus, it appears that a single material with well-defined internal structure (for example nc-Si) can give rise to a pronounced spectral variation when the size is changed within a certain range. In particular, it should be emphasized that, due to this quantum size effect, the spectral properties of nanosized materials can be completely different from those of their bulk counterparts.

Since the radiative recombination takes place between states near the edges of the bands one of the factors determining the width of the PL curve is the variation of the band gap inside a given sample. This is the reason why crystals have rather sharp PL response while amorphous materials exhibit much broader PL bands since they have a distribution of gaps. Thus, it follows that in amorphous materials only those locations can contribute to the PL where the gap is smaller than the energy of the exciting photon. Therefore, it is very important to measure the PL spectra with exciting photons of sufficiently high energy. When the excitation is made with photons that are too low in energy, the PL spectra may not be representative of the material.

In Fig. 2, we have plotted the band gaps of various materials made from Si and/or C. The grey area marks the energy range where the maximum positions of the ERE bands were found. In the amorphous materials, a-C:H and a-SiC:H, the band gap is determined by the degree of sp^3 hybridization of the carbon atoms and by the concentration of C atoms, respectively. Depending on these values, the band gaps cover rather large ranges including the region of the ERE. However, it is also noted that the corresponding materials will exhibit PL outside the ERE range when the sp^3 hybridization (or the silicon content, respectively) does not have the proper value.

The crystalline materials are characterized by rather distinct band gaps. For SiC we have drawn a bar from 2.4 to 3.3 eV, to take into account the different crystalline modifications (e.g. β-SiC: 2.4 eV and α-SiC polytypes: 3.0−3.3 eV). Bulk silicon is represented by the solid circle at 1.17 eV. The variation of the band gap, as a result of the quantum confinement just discussed, is visualized

by the arrow pointing to the right. For carbon the reduction to the nanometer scale will also lead to higher band gaps. As has been shown recently (Lonfat et al. 1999), carbon clusters with a diameter of 1.5 nm have a band gap of 0.65 eV. The consideration of quantum confinement for crystalline SiC will also result in larger band gaps, but this effect has not been considered here since the band gaps are too large anyway.

When discussing the materials presented in Fig. 2 in view of possible carriers for ERE, at first glance three interesting candidates seem to evolve, namely a-C:H, a-SiC:H, and crystalline silicon when its size is reduced to the nanometer scale (nc-Si). Therefore, we have concentrated our investigations on these three materials. With the data obtained, we will show that, of these three materials studied, only nc-Si complies with the constraints imposed by the astronomical observations.

3. Experiment

The apparatus that is schematically shown in Fig. 3 was specifically designed to measure not only the PL spectra of the various materials under discussion but also their PL yields. It essentially consists of a Nd:YAG laser whose fourth harmonic (266 nm) is used to excite the samples, a small vacuum chamber ($p \leq 10^{-6}$ mbar) into which the sample is placed, and, finally, a monochromator with photomultiplier. In order to determine the PL yields quantitatively, the transmission of the optics was carefully measured using a Cary 1 spectrophotometer. Furthermore, the wavelength-dependent detection efficiency of the setup was calibrated by means of a tungsten ribbon lamp whose temperature was determined with a pyrometer. All results presented here were obtained with an excitation wavelength of 266 nm, corresponding to a photon energy of 4.66 eV. This high photon energy was chosen because it is well above the band gap of all materials studied (see Fig. 2) and because the ERE is observed in astronomical objects where UV photons are prevailing. The laser beam is focused on the sample to a 1-mm-diameter spot, the fluence being 1 μJ/cm^2, and the entire excited area is imaged on the 2-mm-wide entrance slit of a 19-cm monochromator. Finally, the dispersed photoluminescence is detected by a photomultiplier with multi-alkali cathode that is sensitive only to wavelengths below 830 nm. The laser power is determined outside of the vacuum chamber using a quartz window as beam splitter and a calibrated UV photodiode.

Since all optical components and the geometry of the setup are well defined, we can calculate the number of UV photons falling on the sample, and, from the measured absorptivity and photoluminescence intensity (per solid angle), we can quantitatively determine the PL quantum yield (η) which is equal to the total number of emitted PL photons divided by the number of UV photons absorbed by the sample. The absorption of the nc-Si samples at the laser frequency was routinely measured by mounting them in front of the same UV photodiode.

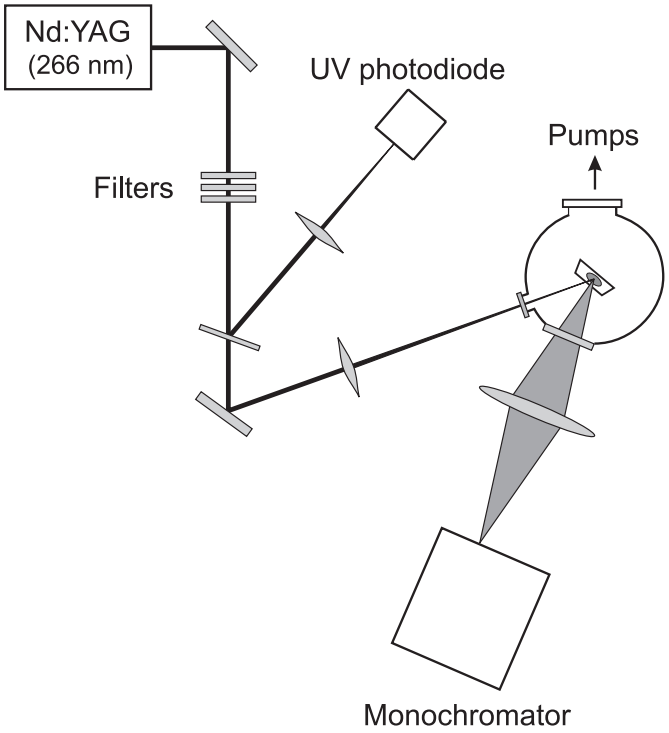

Fig. 3. Schematic view of the experimental setup used to obtain calibrated PL spectra. The optical components are explained in the text.

All other samples were optically thick at 266 nm and thus, we assume that they absorb 100% of the incoming radiation. The proper calibration of the system was confirmed by measuring the fluorescence yield of a solution of Rhodamine 6G that is known to be 95% (Kubin & Fletcher 1982; Georges et al. 1996). Another cross check was provided by the porous silicon samples whose PL yields were determined independently (Vial 1999).

As was stated in the introduction, our study focused only on solid state materials. Five different kinds of samples were investigated, all of them being made of carbon and/or silicon: Natural coals, amorphous hydrogenated carbons (a-C:H), amorphous hydrogenated silicon carbides (a-SiC:H), porous silicon (p-Si) and silicon nanocrystals (nc-Si). Table 1 gives an overview of all samples studied, together with their characteristic properties. The last five columns report the results of the present PL studies.

Coal samples are classified according to the relative proportion of carbon to hydrogen, which is related to their degree of maturation and graphitization. Maturer samples contain less hydrogen and are more graphitic-like (Papoular et al. 1996).

The a-C:H and a-SiC:H samples were produced at the Ecole Polytechnique in Palaiseau by plasma-enhanced chemical vapor deposition (PECVD). The film thicknesses were between 1 and 3 μm. For a-C:H, CH_4 or C_3H_8 was used as precursor gas (Heitz 1998). Depending on the conditions in the CVD reactor, a complete set of samples can be obtained ranging from materials where the carbon is almost only in the sp^2 conformation up to materials where

Table 1. PL and characteristic properties of the different samples studied.

Type	Characteristic property	PL properties				
		λ_{max} (nm)	$\Delta\lambda$ (nm)	ΔE (eV)	η_{PL}	$\eta_{PL}^{corrected}$
Coal	[H]/[C]					
	0.45	500	325	1.51	5×10^{-7}	
	0.58	500	395	1.52	6×10^{-7}	
	0.76	680	470	1.81	2×10^{-6}	
	0.85	490	380	1.65	5×10^{-6}	
a-C:H	gap (eV)					
	1.5	515	280	1.84	1×10^{-5}	
	1.9	575	250	0.98	5×10^{-5}	
	2.1	605	250	0.87	9×10^{-5}	
a-$Si_{1-x}C_x$:H	x					
	0.37	510	150	0.73	1.5×10^{-2}	
	0.25	780	260	0.55	2×10^{-3}	
	0.15	∼900	250	0.35	$\sim 1 \times 10^{-4}$	
p-Si	porosity (%)					
	70	760	150	0.33	1.4×10^{-2}	
	80	700	160	0.41	3.2×10^{-2}	
nc-Si	diameter (nm)					
I	3.65	660	140	0.40	1×10^{-2}	9×10^{-2}
	3.92	750	165	0.38	1.3×10^{-1}	9.4×10^{-1}
	4.95	800	170	0.29	2×10^{-2}	7.4×10^{-2}
II	3.44	680	190	0.51	8.8×10^{-2}	1
	3.46	610	165	0.53	1.6×10^{-2}	1.7×10^{-1}
	3.86	820	180	0.34	1.3×10^{-1}	9.7×10^{-1}
	3.88	710	155	0.40	$\geq 1.5 \times 10^{-1}$	1.1
	4.05	750	150	0.35	$\geq 5.7 \times 10^{-2}$	$\geq 3.9 \times 10^{-1}$
	4.45	800	145	0.28	1.8×10^{-1}	1
III	2.8	635	115	0.32	$\geq 1 \times 10^{-2}$	$\geq 3 \times 10^{-2}$
	3.2	725	145	0.34	7.7×10^{-2}	9.5×10^{-1}
	3.6	∼860	170	0.29	1.1×10^{-1}	1
	4.8	≥900	∼200	0.27	2.5×10^{-3}	1×10^{-2}

it is almost exclusively sp^3. As discussed in Sect. 2, the band gap is determined by the degree of sp^3 hybridization. Thus, in the present study, it ranges from 1 to 2.1 eV (see Table 1). The a-SiC:H samples were prepared from the precursor gases, silane (SiH_4) and methane (CH_4), supplied in different proportions so as to obtain a set of samples with different ratios of carbon to silicon and thus different band gaps (Tessler & Solomon 1995).

Porous silicon samples were obtained from Vial and coworkers from the University of Grenoble (Vial et al. 1992). They were made by electrochemically etching Si wafers with hydrofluoric acid (HF) and oxydizing them at high temperature. The porosities were determined to be 70% and 80%, respectively.

The major and more difficult part of the present study was devoted to the synthesis of nanocrystalline silicon particles and the characterization of their PL behavior. Well-characterized thin films of non-interacting silicon nanoparticless were produced in Göttingen by pulsed CO_2 laser pyrolysis of silane in a dedicated gas flow reactor and molecular beam apparatus. This apparatus and the characterization techniques used have been thoroughly described before in Ehbrecht et al. (1995), Ehbrecht et al. (1997), Ehbrecht & Huisken (1999), and Ledoux et al. (2000a). The reader is referred to these papers for a complete description of the method. Here we will only summarize the main results. In contrast to porous silicon that is also nanocrystalline but made from bulk silicon, the silicon nanoparticles are grown in the gas phase by condensation of a saturated vapor of silicon atoms at elevated temperature (≥1300 K). The as-prepared Si clusters are extracted from the flow reactor to form a pulsed molecular beam of non-interacting particles. Since their velocity is strongly correlated with their size (the smaller

nanoparticles are faster than the larger ones), they can be selected according to their size by using a simple molecular beam chopper (Ehbrecht et al. 1997; Ehbrecht & Huisken 1999). Thin films of size-selected neutral silicon nanoparticles were then deposited at low energy on various substrates placed into the beam. When the substrate is not in place the particles can proceed into another chamber where they are analysed by time of flight mass spectrometry (TOFMS). The size distribution determined in the beam by TOFMS was further checked ex situ by atomic force microscopy (AFM) of a low coverage deposit. The two size distributions were found to be completely consistent in the small size regime (between 0 and 10 nm). As a result, we could conclude that TOFMS is very well suited to determine the size distribution of nanoparticles on the substrate (Ledoux et al. 2000a). The AFM further revealed that a few larger silicon particles with sizes above 10 nm were also present which were not detected by the TOF mass spectrometry. although the abundance of the undesired particles is low (less than 10% in number), they could play a non-negligible role in the determination of the PL yield, since these big particles have rather large absorption cross section (for a detailled study of this effect the reader is referred to Ledoux et al. 2000a). In the present study, we have investigated three sets of nc-Si samples that were prepared under the same conditions but at different dates (designated by I–III in Table 1). All of these samples suffer from the contamination by undesired particles larger than 10 nm, that has to be taken into account in the PL yield analysis. Since the presence of these big particles is a result of the mode of production they are not present in the other samples (a-C:H, a-SiC:H and porous silicon) studied in this work.

It was said before that the PL yield depends on the competition between radiative and non-radiative recombination via defects. Since dangling bonds are very common non-radiative defects it is important that the surfaces of the nanocrystals are perfectly passivated. For the silicon nanoparticles studied here, a natural passivation was achieved by exposing the samples for a few days to the ambient air. This oxidation process was studied by high resolution transmission electron microscopy (HRTEM). It was found to be self limiting, leading, after 2 months, to a final oxide layer whose thickness is approximately 10% of the total particle diameter (Hofmeister et al. 1999). No further oxidation was observed during a period of 2 years.

4. Experimental results

For all materials studied, the measured PL spectra show a single, broad, and structureless band that can be described in terms of three characteristic parameters: peak position ($\lambda_{\max}$), full width at half maximum of the PL curve ($\Delta\lambda$), and the integral intensity of the PL signal or, when it is related to the number of photons absorbed, the PL yield (η_{PL}). These data are collected in Table 1.

With yields lower than 5×10^{-6}, coal samples show the weakest photoluminescence. The yield decreases as the hydrogen content decreases. The bands are extremely wide (larger than 320 nm or 1.5 eV), and thus, the determination of the peak positions is not very precise. In any case, $\lambda_{\max}$ remains below 680 nm.

The a-C:H samples feature somewhat higher but still quite low PL efficiencies ($\eta_{\mathrm{PL}} \leq 10^{-4}$). Again the bands are broad (≥ 250 nm), and they do not reflect well-defined lineshapes. The peak positions are estimated to lie in the 500 to 600 nm range. Compared with the literature data, the present results reproduce the tendency for the efficiency to increase when the band gap of the material increases (Xu et al. 1993) and to exhibit a rather large PL range (for a review see Cernogora 1997). This range is sensitive to the excitation wavelength (Vasil'ev et al. 1990) in so far as the PL spectra are truncated at the blue side if the excitation energy is not high enough (see the discussion in Sect. 2).

Amorphous hydrogenated silicon carbide (a-SiC:H) shows photoluminescence over a very wide range. With increasing carbon content, the PL yield varies monotonically from 10^{-4} to 1.5×10^{-2} (see Fig. 5) while the peak position moves from the near infrared to 510 nm. At the same time, the width of the PL bands varies from 250 to 150 nm. Our observations agree nicely with the results of other laboratories who have conducted extensive studies on this material (Siebert et al. 1987; Liedtke et al. 1989; Tessler & Solomon 1995).

In contrast to the samples just discussed, porous silicon and silicon nanocrystals are characterized by rather high quantum yields ($10^{-2} \geq \eta_{\mathrm{PL}} \geq 0.18$), giving rise to a strong photoluminescence that, in many cases, is clearly visible to the naked eye (Huisken et al. 1999b; Huisken et al. 2000). The bandwidths are also quite narrow ranging from 115 up to 200 nm. Finally, the range of wavelengths where we found the PL maxima is between 600 and 900 nm.

As we have discussed in Sect. 2, there is a correlation between the peak of the PL curve and the size of the silicon nanoparticles (or the porosity of p-Si) as a result of the quantum confinement. In order to clearly demonstrate this effect, it was necessary to produce samples of nc-Si with rather narrow size distributions as has been described in Sect. 3. In Fig. 4 we present the size distributions of the two samples characterized by average diameters of 3.44 and 4.95 nm, respectively, and the corresponding PL curves. The film with the smaller particle size (3.44 nm) produces a PL curve that has its maximum at 680 nm while the other sample with $\sim$5 nm particles gives rise to a PL curve with a maximum around 800 nm. As has been shown in a very recent publication (Ledoux et al. 2000a), the measured PL maxima correlate nicely with the particle diameter in accordance with the quantum confinement law (Delerue et al. 1993) (see also Sect. 2).

The yields, η_{PL}, listed in the 6th column of Table 1 are the external yields as they were determined just by taking into account the overall absorption of the samples. As explained before, the nc-Si samples suffer from

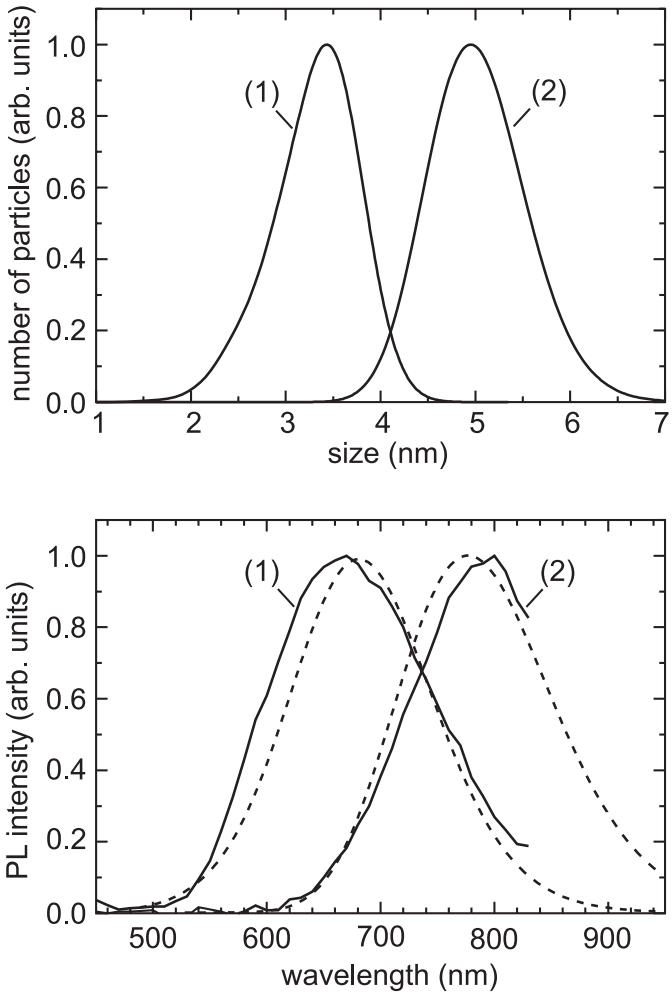

Fig. 4. Size distributions of two different samples of silicon nanoparticles as determined by TOFMS (upper panel) compared with the PL curves measured for the same samples (solid curves of bottom panel). The dashed curves represent synthetic spectra based on the measured size distributions (for details see last paragraph of Sect. 4).

contamination by particles larger than 10 nm. These particles are much less sensitive to the confinement effects than the smaller nanocrystals, and they are expected to luminesce more in the infrared with a very low efficiency. Therefore they will not contribute to the PL range of interest here but they will absorb a substantial portion of the incoming light. Taking into account this effect, we determined corrected internal yields for the small nanocystals $\eta_{\mathrm{PL}}^{\mathrm{corrected}}$, that are listed in the last column of Table 1. Now it appears that, for most samples, the corrected PL efficiencies are close to 1. For the largest particles studied here ($\sim$5 nm), the yield seems to be somewhat lower, but further investigations should be carried out to corroborate this trend.

In our recent detailed study on the PL properties of size-selected Si nanoparticles (Ledoux et al. 2000a), we have shown that the wavelength dependence of the photoluminescence can be very well understood on the basis of the quantum confinement model and that the experimental observations comply with the theoretical results of Delerue et al. (1993). Moreover, using the theoretical correlation ($E_{\mathrm{PL}} \sim d^{-1.39}$) and the measured size distribution of the silicon nanoparticles, we were able to model the PL response of the corresponding sample. Indeed, as is shown in Fig. 4, the agreement between measurement and model calculation is rather good. Conversely, for any given PL curve resulting from silicon nanoparticles, we can predict the size distribution of the nanoparticles in the sample responsible for the photoluminescence (Ledoux et al. 2000a).

5. Comparison with astrophysical data

5.1. Comparison of characteristic parameters

In order to compare the laboratory measurements with the astronomical observations, we have plotted the two characteristic parameters, PL yield and PL bandwidth, as a function of the PL peak wavelength. These two diagrams are depicted in Figs. 5 and 6. The grey-shaded areas indicate the variation of peak positions, efficiencies, and widths of the ERE bands (as a function of wavelength) observed so far. The lowest limit for ERE efficiency was set by Smith et al. (1999) to 6×10^{-4}, but the constraint resulting from the observation of ERE in the DISM pushes this limit to 10^{-1} if we consider that the same material is responisble for all ERE observations. As can be seen, all data points related to nc-Si (filled circles) and p-Si (filled squares) reflect perfectly the observed general constraints on these three PL parameters (except the one at 900 nm). As in ERE observations, the PL spectra of these materials are rather narrow, strictly confined to the red region of the electromagnetic spectrum (i.e. with a peak between 600 and 850 nm), and demonstrate high emission efficiencies. In the laboratory, these last two characteristic properties are directly evidenced by the bright and intense red luminescence observed with naked eyes when these samples are exposed to 254-nm-radiation from a simple laboratory UV lamp. In contrast, no visible light is detected for the other samples considered here, reflecting the 2 or 3 orders of magnitude smaller PL yields for these materials.

The results for the carbon-based samples (coal, a-C:H, and a-SiC:H) fall clearly outside the limits imposed by the astronomical observations in terms of PL peak maximum and yield (Fig. 5). Since it was our intention to study samples with electronic gaps falling into the ERE energy range, the present results do not reflect the full range of the PL behavior of these materials. However, even if we take into account all the results published so far, no better agreement is observed. For example, a-C:H samples with relatively high PL yields ($\eta \sim 10^{-3}$) can be obtained. Such samples belong to a subclass of the wide a-C:H family usually referred in the literature to as "polymer-like" or "soft a:C-H". They are characterized by a large content of hydrogen and sp^3 carbon, and, as a consequence, their gap is rather large and their photoluminescence peaks in the blue. But, up to now, such blue PL bands have not been

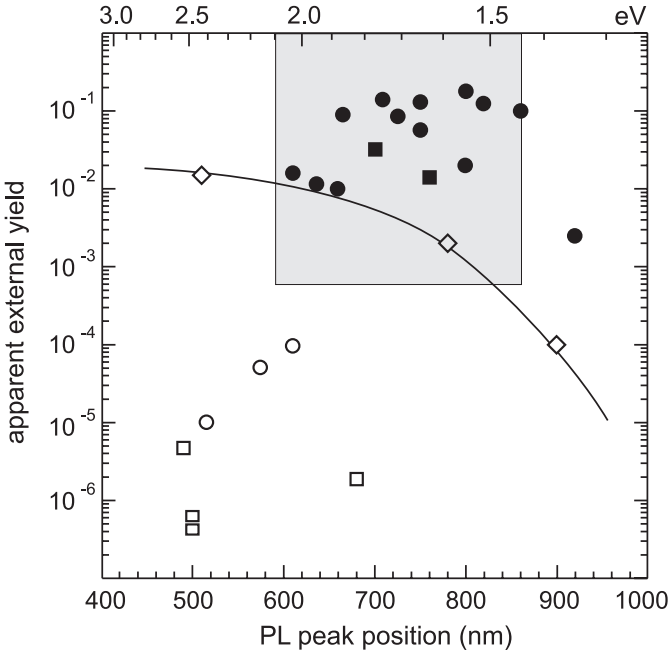

Fig. 5. Correlation diagram showing the measured photoluminescence yields as a function of the peak position of the PL band for the different samples studied: coal (□), a-C:H (○), a-SiC:H (◇), p-Si (filled squares), and nc-Si (filled circles). The range of peak wavelengths and yields known from astrophysical observations is indicated by the grey-shaded area. The lowest yield of 6×10^{-4} was reported by Smith et al. (1999).

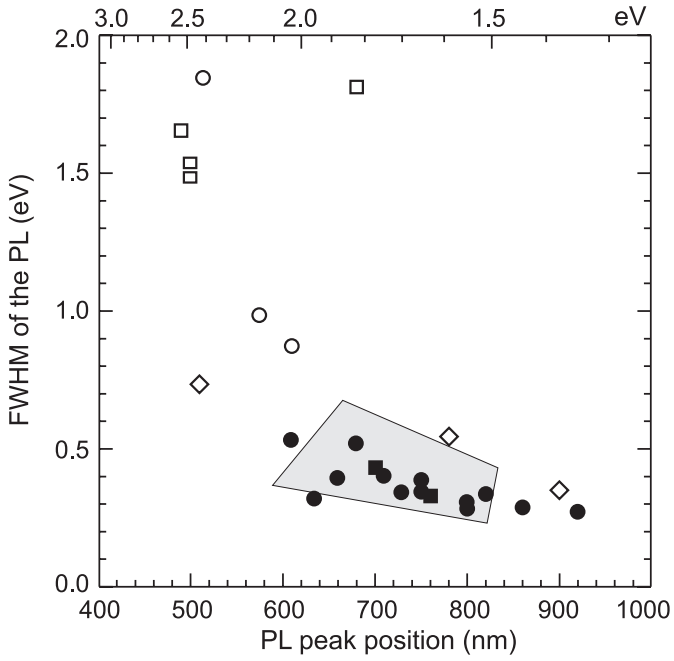

Fig. 6. Correlation diagram of measured widths (*FWHM*) and maximum positions of the measured PL bands: coal (□), a-C:H (○), a-SiC:H (◇), p-Si (filled squares), and nc-Si (filled circles). Again the grey-shaded area indicates the variation of the ERE observations.

reported from astronomical observations. Now, starting from soft a-C:H, a closure of the gap can be achieved by increasing the content of sp^2 carbon, either by changing the synthesis conditions or by post-treatment. As a result, the PL shifts towards the ERE range, but this goes together with a drastic decrease in the PL efficiency. Hence, this material is not at all a suitable candidate for ERE.

As far as the a-$Si_{1-x}C_x$:H samples are concerned, their PL maxima span a large range of wavelengths that extends from the near IR to the blue. Our measurements are in good agreement with the results of Tessler & Solomon (1995), shown in Fig. 5 as the solid curve. It happens that only samples with a fraction of carbon in the range $0.2 \leq x \leq 0.3$ peak at suitable wavelengths. Such a limited range would be difficult to justify in space. Moreover, the yield is too low to be compatible with the DISM constraint. The highest yield reported here in the ERE range is 0.2%. While this result was obtained at room temperature, it is well known that the PL yield of a-SiC:H increases when the temperature is lowered (Tessler & Solomon 1995). However, for samples which show PL in the ERE range this increase is rather modest. It does not exceed 0.3% at 77 K. So from the yield measurements alone this material could only explain a few observations where very low yields are needed.

Figure 6 clearly shows that, independent of the constraints on peak position and efficiency, the PL bands of the amorphous materials are far too broad compared to the ERE bands. These large bandwidths are due to their amorphous, i.e. disordered, structure. This characteristic property provides a strong argument against a-C:H as a candidate carrier for ERE. In this context, it is worthwhile to comment on several PL measurements reported in the past (Witt & Schild 1988; Webster 1993) and more recently (Furton et al. 1999) in the astrophysical literature and which were obtained with excitation wavelengths in the visible range, mostly using the 488-nm line of an Ar^+ laser. These measurements have to be viewed with great care when discussing the PL spectroscopy of a-C:H in the context of the ERE problem. Indeed, with such low excitation energy, the high energy part of the PL spectral distribution could be truncated, resulting in an apparent narrower bandwidth and a peak position shifted too much to the red. This underlines the importance of using UV excitation if one wants to study the PL of possible candidate carriers. In particular, this is true since the ERE only occurs in regions where UV radiation is prevalent.

To conclude this section, we state that coal, a-C:H, and a-SiC:H samples have difficulty in simultaneously fulfilling all three constraints just discussed (peak position, yield, and width). In contrast, the PL behavior of nanocrystalline silicon (p-Si and nc-Si) demonstrates very good agreement with the general properties of ERE observations. So, from the comparative study of these three characteristic parameters alone, nanostructured crystalline silicon emerges as the best candidate to explain ERE.

5.2. Comparison of the spectroscopy

Direct comparisons between laboratory-measured PL curves of size-selected silicon nanoparticles and astronomical ERE spectra have already been published by Ledoux et al. (1998, 2000b). In Fig. 7, we present two additional comparisons between laboratory data and ERE observations for which we succeeded in achieving rather convincing agreement (Figs. 7a and e). The parameters of the corresponding size distributions of the Si nanoparticles as determined from the TOF measurements are given in the figure caption. These spectroscopic comparisons provide rather good estimates for the size distributions of the photoluminescent particles in the astronomical objects under consideration. However, it should be mentioned that the good agreement is in a certain manner accidental, and, in some cases, better agreement could be conceivable.

To go further into the reproduction of *all* ERE observations and to obtain a more general description of the astronomical observations, we make use of the model calculations discussed in Sect. 4. We have applied this method to fit all ERE spectra that have been published so far. For each individual ERE source investigated, Table 2 gives the size distribution of silicon nanoparticles that provides the best agreement between the astronomical feature and the simulated spectrum. Illustrations of the spectral adjustments are also presented in Fig. 7 (panels b–d). In order to reproduce the entire range of ERE positions and profiles, the mean diameter of nc-Si particles has to be varied between 2.5 and 6 nm. These results illustrate that a rather limited range of size distributions of the luminescent grains can account for all the diversity of ERE observations, irrespective of whether they were made in different objects or within a given object.

When we compare the ERE observations from different locations of the same object, we notice that there is a clear tendency of the ERE to shift to the red when getting closer to the illuminating star. For example, in the case of the Red Rectangle, the ERE peak shifts by 130 nm as a function of the position in the nebula. In our model, this progressive red-shift corresponds to an increase of the mean size of the nc-Si particles from 2.6 to 4.3 nm. This behavior is illustrated in Fig. 8 where we have plotted the mean size of the Si nanoparticles responsible for the ERE as a function of the distance from the illuminating star. It is seen that a modest variation of the size with the distance from the exciting source is able to explain the entire set of ERE spectra observed in the Red Rectangle.

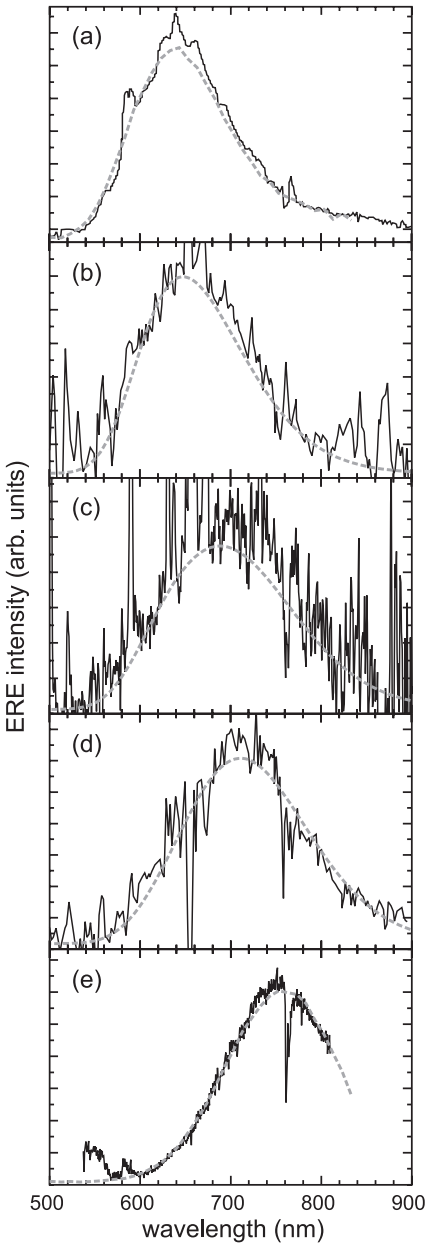

Fig. 7. Comparison between five observations of ERE in different objects and experimental (**a)** and **e)**) or synthetic (**b)**–**d)**) PL spectra of Si nanocrystallites. The observations are from **a)** Red Rectangle (Witt & Boroson 1990), **b)** NGC 2023 (Witt & Boroson 1990), **c)** M 82 (Perrin et al. 1995), **d)** NGC 2327 (Witt 1988), and **e)** Red Rectangle (Rouan et al. 1995). The average particle sizes for the experimental PL spectra are 2.71 nm **a)** and 4.5 nm **e)**. The synthesized spectra are based on log-normal size distributions with $< d > = 2.85$, 3.3, and 3.6 nm and *FWHM*'s of 1.08, 1.6, and 1.45 nm (**b)**–**d)**), respectively.

6. Discussion

Since nc-Si grains seem to be a good carrier candidate for the Extended Red Emission we would like to discuss in more detail the consequences of this model. In particular, we would like to discuss this in light of the different observationally established constraints listed in the introduction.

We have shown that there is clearly a striking analogy between the PL behavior of nc-Si particles measured in the laboratory and the ERE properties. Indeed, the photoluminescence of nc-Si is quite strong and confined to the red region of the electromagnetic spectrum (above 600 nm) as it is in the sky. This ERE spectral characteristic would then be a direct consequence of the quantum confinement

Table 2. Parameters of the log-normal size distributions used to model different astronomical observations.

Object	Observations			Fit parameters		
	ERE_{max} (nm)	*FWHM* (nm)	Reference	d_{max} (nm)	σ	Δd (nm)
M 82 postion 1	665	190	(Perrin et al. 1995)	2.8	0.3	2.02
M 82 postion 2	690	170	(Perrin et al. 1995)	3.3	0.2	1.56
M 82 postion 3	700	190	(Perrin et al. 1995)	3.5	0.25	2.1
M 82 postion 4	700	190	(Perrin et al. 1995)	3.5	0.27	2.25
NGC 2247	670	160	(Witt & Boroson 1990)	3.15	0.17	1.27
NGC 2327	715	165	(Witt 1988)	3.6	0.17	1.46
VdB43	650-700	212	(Rouan et al. 1995)	3.3	0.4	3.2
NGC 2023, 62″ ENE from star	645	135	(Witt & Boroson 1990)	2.85	0.16	1.08
NGC 2023, 84″ ENE from star	670	135	(Witt & Boroson 1990)	3.1	0.11	0.8
NGC 2023	780	160	(Rouan et al. 1995)	5.75	0.25	3.42
NGC 7023	675	155	(Gordon et al.2000)	3.1	0.16	1.19
Red Rectangle 1.5″ S from star	765	150	(Rouan et al. 1995)	4.27	0.14	1.42
Red Rectangle 2″ S from star	755	145	(Rouan et al. 1995)	4.17	0.14	1.38
Red rectangle 5″ S from star	700	130	(Rouan et al. 1995)	3.7	0.12	1.05
Red Rectangle 6″ S from star	660	160	(Witt & Boroson 1990)	3	0.2	1.42
Red Rectangle 10″ S from star	635	125	(Witt & Boroson 1990)	2.6	0.2	1.21
Red Rectangle 10″ N from star	635	115	(Schmidt et al. 1980)	3.0	0.1	0.72
NGC 7027	705	145	(Furton & Witt 1990)	3.5	0.11	0.92
NGC 6790	760	175	(Furton & Witt 1992)	4	0.2	1.9
Sh 152 position 1	705	150	(Darbon et al. 1999b)	3.2	0.15	1.12
Sh 152 position 3	735	150	(Darbon et al. 1999b)	3.5	0.15	1.23
Orion B4	775	205	(Perrin & Sivan 1992)	3.6	0.29	2.5
NGC 7635	770	210	(Sivan & Perrin 1993)	5	0.4	4.86

effect which makes the band gap of silicon progressively wider, starting from the near IR (i.e. 1.17 eV, the gap value of bulk silicon) and extending progressively deeper into the visible region when the particle size decreases.

6.1. Size distribution of silicon nanoparticles

As illustrated in Sect. 5.2, the range of observed ERE wavelengths points to populations of nc-Si grains with average diameters ranging between 2.5 and 6 nm (i.e. 400−6000 atoms). Even if we consider the tails of the size distributions, we finally obtain a size range extending from 1.5 to 12 nm (values where the size distributions have dropped to 1/10 of the maximum amplitude). The quoted sizes fall precisely into the range of sizes for which the spatial confinement becomes extremely important and the PL efficiency is strongly enhanced. Hence, in accordance with the detection of ERE photons, only very small nc-Si grains are efficient emitters and show red luminescence.

Obviously, the size distributions entering our fits only reflect the size distributions of the luminescent particles and are not representative of the entire population of nc-Si grains. In other words, a larger distribution may be present in the astronomical object, but only the PL of the smaller particles is detected. Indeed, for grains with diameters larger than 6 nm, the PL yield begins to decrease, simply because the probability of radiative recombination is reduced.

Up to now, we have only assumed that the PL arises from single non-agglomerated nanoparticles. However, it could also be possible that the luminescent particles are considerably larger provided that they are composed of individual nanocrystals of the proper size just discussed. This requires that they are separated by an energy barrier in the form of an oxide, a host matrix, or a vacuum, making these agglomerates comparable to porous silicon, as far as their PL properties are concerned.

The limit on the other side of the size distribution is less clear. Indeed, the theory predicts that, for grains smaller than 2.5 nm, the PL band will be shifted into the green-yellow region. We did not succeed to observe such green-yellow photoluminescence in the laboratory. An obvious explanation could be that these very small grains (<400 atoms) are not efficiently produced in the laser pyrolysis experiment. We may imagine that this is peculiar to the cluster growth mechanism. However, Akcakir et al. (2000) have reported blue luminescence from hydrogen-passivated nc-Si of about 1 nm in size. It could also be an

indication of the stability domain of free crystalline silicon clusters. An alternative explanation could result from the process of surface oxidation. The passivation of surface dangling bonds with oxygen atoms leads to the formation of an amorphous oxide shell surrounding the crystalline Si core. Hofmeister et al. (1999) have shown that the oxidation of spherical Si nanoparticles is a size-dependent self-limiting process. The strong stress due to the curvature of the interface makes it difficult to achieve a perfect passivation of the smallest grains. Thus, non-radiative interfacial centers, which quench the PL, may still be present. On the other hand, one could also imagine that small crystalline silicon clusters will be completely oxidized when they are exposed to oxygen, so that the crystalline core is completely destroyed. In this context, it is interesting to note that, for a crystalline core consisting of 400 Si atoms (d = 2.5 nm), already 60% of the atoms are located at the interface so that a drastic change of the PL properties is quite likely. Finally, we would like to mention the combined theoretical and experimental study of Wolkin et al. (1999) who showed that oxygen-passivated silicon quantum dots approach a saturation value of 2.2 eV for their band gap (corresponding to a PL maximum at 570 nm) when their size becomes smaller than 2.5 nm.

6.2. Width of PL band

As evidenced in Fig. 6, the narrowest ERE feature observed so far has a bandwidth of about 0.23 eV. This value compares very well with the "intrinsic" bandwidth of 0.25 eV that we derived from our analysis of the PL properties of nc-Si particles (Ledoux et al. 2000a). This minimum bandwidth is rather broad and we could attribute it to an inhomogeneous broadening mechanism. It is associated with the small variations of the lattice parameter of the Si core observed by HRTEM (Hofmeister et al. 1999). Even if the core diameter is the same, different particles may have experienced different degrees of oxidation resulting in different stress on their core and thus different lattice parameters. It follows that the observed variations of the ERE bandwidth are probably the result of a similar inhomogeneous broadening effect convoluted with the size distribution of the luminescent particles.

6.3. Variation of ERE characteristics with radiation field

A general trend is observed when comparing ERE features from one object to another. The reddest ERE bands are observed in environments powered by strong radiation field intensities, like HII regions and planetary nebulae, whereas reflection nebulae exhibit bluer peaks. The bluest ERE band is observed in the diffuse ISM at about 600 nm (Gordon et al. 1998). A similar behavior is reported from individual objects as a function of the distance from the nearby exciting source: with increasing distance, the ERE is progressively blue-shifted. Finally, very far from the star, the spectral position is close to the one observed in the diffuse ISM. Hence, the ERE emission seems to be sensitive to the UV photon density. We have shown that the wavelength variations of the ERE can be explained by different size distributions of the Si nanoparticles. Due to the strong dependency of the PL maximum on the size, only slight variations of the order of 1 to 2 nm in the average diameter of the particles can explain the large range of ERE observations.

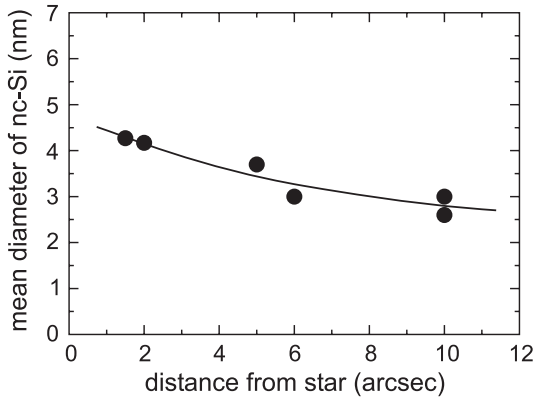

Fig. 8. Variation of the mean size of the nc-Si size distribution used to model the ERE bands as a function of the distance from the illuminating source in the Red Rectangle nebula. The solid curve has been drawn to guide the eyes.

One possible explanation for the observed size variations could be some process of photo-destruction in strong radiation fields, as proposed by Witt et al. (1998). In harsh environments, small grains would be more easily destroyed, resulting in a shift of the size distribution of the luminescent particles towards larger sizes. When subjected to milder radiation fields, the small grains can survive, thus shifting the ERE maximum towards shorter wavelengths. An alternative explanation could be based on the radiation pressure which would create a depletion of the smaller particles in the vicinity of the exciting star. The competition between gravitation and the radiation pressure force would lead to a segregation of grains with different sizes as a function of their distance from the star.

6.4. Requirements to explain observed ERE intensities

As was shown in the Sect. 4, the yield $\eta_{\rm PL}$ of nc-Si can be as high as 1. Even if we suspect that $\eta_{\rm PL}$ decreases when the particle size is smaller than 2.5 nm or larger than 6 nm, our results provide strong evidence that $\eta_{\rm PL}$ is close to 1 for nc-Si particles in the 2.5−6 nm size regime that corresponds exactly to the ERE wavelength range. Therefore, it is justified to assume that the PL yield of nc-Si particles is always higher than the minimum yield ($\eta_{\rm min}$ = 0.1) required to fulfill the constraint imposed by the DISM observations. It is even higher than the highest required yield reported so far ($\eta_{\rm min}$ = 0.25, Smith et al. 1999). Assuming $\eta_{\rm PL}$ = 1, it follows that nc-Si particles

are responsible for 10% of the UV/visible absorption in the DISM.

With this result in mind, we will now estimate the amount of silicon needed in the form of nc-Si, in order to verify that it does not reach unreasonable values. Fortunately, the average absorption coefficient of silicon in the range between 100 and 550 nm is particularly high ($\alpha_{\rm Si} = 10^6$ cm^{-1}; Theiss 1997). Thus, it is ten times larger than the average absorption coefficient of the dust in the DISM ($\alpha_{\rm DISM}$) that is estimated to be around 10^5 cm^{-1} (Huffman 1977).

Let X be the proportion of nc-Si in the dust by volume, and $\alpha_{\rm ex}$ the average absorption coefficient of the dust, excluding the nc-Si component. Then we can write for a given optical depth d (assuming the same albedo for all the grains)

$$\alpha_{\rm DISM} d = \alpha_{\rm Si} X d + \alpha_{\rm ex}(1 - X)d. \quad (1)$$

The quantity $\eta_{\rm min}$, determined by Gordon et al. (1998) to be 0.1, can be expressed as the product of the yield $\eta_{\rm PL}$ of the material responsible for ERE and its relative absorption of the UV/visible photons ($X\alpha_{\rm Si}/\alpha_{\rm DISM}$). Solving this relation for X, we obtain

$$X = (\alpha_{\rm DISM}/\alpha_{\rm Si})(\eta_{\rm min}/\eta). \quad (2)$$

We note that, the higher $\alpha_{\rm Si}$ and η, the lower is X. Taking $\eta_{\rm PL} = 1$, we obtain $X = 0.01$ for the DISM. Going with this value into Eq. (1), we calculate for the absorption coefficient of the nonluminescent dust $\alpha_{\rm ex} = 9.1 \times 10^4$ cm^{-1}. Thus, $\alpha_{\rm ex}$ is very close to $\alpha_{\rm DISM}$, which means that the average properties of the dust are only slightly changed by introducing the nc-Si particles as a new component. From the X value, a rough estimate of the total mass of nc-Si can be made. Since the density of crystalline silicon (2.4 g cm^{-3}) is not very different from the average density of cosmic dust it follows that the total mass of nc-Si represents 1% of the total mass of depleted interstellar atoms. In conclusion, due to the high UV absorption coefficient and the very high PL conversion efficiency, only a very small fraction of the interstellar dust needs to be in the form of nc-Si particles to account for the observed ERE intensity. Note that the present calculation has been done for the severest constraint, as is provided by the DISM. In most other objects, the constraints are much more relaxed, leading to nc-Si concentrations that can be smaller by one or two orders of magnitude.

Since silicon is an indirect-gap semiconductor its absorption curve shows two pronounced steps corresponding to the indirect and direct gap. The direct gap transition is around 400 nm, in a region where the absorption coefficient decreases by two orders of magnitude (from 3×10^6 cm^{-1} at 250 nm to 10^4 cm^{-1} at 500 nm). This may be the reason why ERE has never been observed near stars with color temperatures lower than 7000 K. For these cool stars the Si nanocrystals will absorb proportionally less of the available photons than all other dust components. Then ERE might be present, but at an undetectable level.

6.5. Other spectroscopic signatures

Another important issue to be discussed here are other possible signatures arising from these silicon nanocrystals. In the UV range, bulk Si has one very small absorption feature around 280 nm, but this structure is smeared out in nanocrystals (see for instance Theiss 1997; Zubko et al. 1999). In the mid-infrared region, it will depend on the kind of passivation of the nanocrystals. The most probable cases are oxygen or hydrogen passivation. In the case of an oxide layer around the nanocrystals, the material should be very similar to our laboratory samples which have an oxide layer with a thickness of about 10% of the total particle diameter (core plus 2× oxide layer). For these samples, we have measured infrared spectra (Huisken et al. 1999a) in the range between 2.5 and 25 μm. The strongest peak appearing in the spectrum is at 9.5 μm. Other very weak peaks are present at 11.8 and 20 μm. Because of the small amount of nanocrystals necessary to explain ERE, only the stronger peak may be observable and only for the most stringent cases in the DISM or in the object where $\eta_{\rm min} = 0.25$ (Smith et al. 1999). The other possible passivation is by hydrogen. In this case, there would be only a monoatomic layer of hydrogen around the surface of the nanocrystals. This is in contrast to the oxygen-passivated samples that are characterized by a thick oxide layer. The peak arising in the IR spectra due to the Si–H bond will be at 4.6 μm, but is expected to be very weak.

Interestingly, in the very near infrared, Gordon et al. (2000) recently discovered two bands at 1.15 μm and 1.5 μm. The second band is attributed by the authors to the photoluminescence of $FeSi_2$, a direct-band gap semiconductor. The first band, however, could be due to silicon nanocrystals since, at low temperature, the recombination of the electron-hole pair on dangling bonds becomes radiative (Hill & Whaley 1996a; Hill & Whaley 1996b; Meyer et al. 1993; Gardelis & Hamilton 1994). The energy (in eV) of the emission $E_{\rm p}$(IR) is then related to the normal photoluminescence energy $E_{\rm p}$(ERE) according to

$$E_{\rm p}({\rm IR}) = 0.43 E_{\rm p}({\rm ERE}) + 0.34. \quad (3)$$

In the case of the observation of Gordon et al. this relation is proved to be correct. It would be interesting to check this correlation also in other objects where ERE is observed and where this second band is present (most probably in cold environments).

It is still difficult to draw any conclusion regarding this subject since we need absolute values for the indices of refraction of nc-Si in the infrared. As for the astrophysical part, it would be interesting to have spatially resolved infrared measurements that could be readily compared with the ERE observations. With these two pieces of information it would be possible to confirm or discard our hypothesis.

6.6. formation of Si nanocrystals

Finally, we would like to discuss on what could be the formation processes of silicon nanocrystals in space. It may be important to describe first a few experiment that have been published and that can give us insight on this process of formation. In the last five years many different ways of producing nc-Si have been discovered. One general method is to produce a material with a stoichiometric excess of Si. After annealing these materials there is a natural formation of nc-Si embedded in the stoichiometric matrix and with sizes comparable with the nanocrystals studied in this work. In this context matrix like quartz (Shimizu-Iwayama et al. 1998; Linnros et al. 1999; Murakami et al. 1999), diamond (Terranova et al. 1999) or phosphosilicates (a mixture of SiO_2 and P_2O_5) (Inoue et al. 1999) have been used. Everytime, the PL associated with the nc-Si has been observed. So as long as silicon atoms will be slightly in excess in a zone it's most probable that there will be formation of nanocrystals. Gail & Sedlmayr (1999) recently calculated that the formation of SiO_2 in stellar outflow was a two step process with, at first, the formation of solid SiO and then the reaction of it with water to form SiO_2. However, at the temperature considered in this work ($\sim$1000 K) we know from laboratory experiments (Kachurin et al. 1997) that within minutes there is formation of silicon nanocrystals in the suboxide. Again, one would like to know the spectral properties of these materials doped with nc-Si in the infrared, in order to check whether there is any correlation of the ERE observations with these spectral signatures.

7. Conclusion

From the study of different solid materials made from silicon and carbon, one interesting candidate to explain ERE has emerged: silicon nanocrystals. An attractive feature of the present model is that a single carrier can explain all ERE observations known so far. The spectral variations can be explained just by invoking different size distributions of silicon nanocrystals. The sizes discussed here are known to be present in the interstellar grains. It should be mentioned that, for the first time, quantum effects on optical properties of solids are used to explain an interstellar observation. In the case where ERE is most intense in relation to the intensity of the exciting radiation field (the diffuse interstellar medium), the amount of material needed to be in the form of silicon nanocrystals is only 1% of the total mass of the dust. It is still an open question in what form the Si nanoparticles may be present in order to have the dangling bonds fully saturated. Therefore, it is important to know the exact optical properties of nanocrystalline silicon with various kinds of passivation. This information should be measured from the infrared to the UV and as a function of the size of the particles.

Acknowledgements. We are very grateful to Adolf Witt for fruitful discussions and comments. F. H. acknowledges the support of the Deutsche Forschungsgemeinschaft. This work was further supported by PROCOPE, a bilateral cooperation between France and Germany.

References

Akcakir, O., Therrien, J., Belomoin, G., et al. 2000, Appl. Phys. Lett., 76, 1857
Cernogora, J. 1997, Phys. Stat. Sol. (b), 201, 303
Cohen, M., Anderson, C. M., Cowley, A., et al. 1975, ApJ, 196, 179
Cullis, A. G., Canham, L. T., & Calcott, P. D. J. 1997, Appl. Phys. Rev., 82, 908
Darbon, S., Perrin, J.-M., & Sivan, J.-P. 1999a, A&A, 348, 990
Darbon, S., Zavagno, A., Perrin, J.-M., et al. 1999b, A&A, submitted
Delerue, C., Allan, G., & Lannoo, M. 1993, Phys. Rev. B, 48, 11024
d'Hendecourt, L. B., Leger, A., Olofsson, G., & Schmidt, W., 1986, A&A, 170, 91
Duley, W. W. 1985, MNRAS, 215, 259
Ehbrecht, M., Ferkel, H., Smirnov, V. V., et al. 1995, Rev. Sci. Instrum., 66, 3833
Ehbrecht, M., & Huisken, F. 1999, Phys. Rev. B, 59, 2975
Ehbrecht, M., Kohn, B., Huisken, F., Laguna, M. A., & Paillard, V. 1997, Phys. Rev. B, 56, 6958
Feng, Z. C., & Tsu, R. 1994, Porous Silicon (World Scientific)
Furton, D. G., Laiho, J. W., & Witt, A. N. 1999, ApJ, 526, 752
Furton, D. G., & Witt, A. N. 1990, ApJL, 364, L45
Furton, D. G., & Witt, A. N. 1992, ApJ, 386, 587
Gail, H.-P., & Sedlmayr, E. 1999, A&A, 347, 594
Gardelis, S., & Hamilton, B. 1994, J. Appl. Phys., 76, 5327
Georges, J., Arnaud, N., & Parise, L. 1996, Appl. Spectrosc., 50, 1505
Gordon, K. D., Witt, A. N., Rudy, R. J., et al. 2000, ApJ, 544, 859
Gordon, K. G., Witt, A. N., & Friedmann, B. C. 1998, ApJ, 498, 522
Heitz, T., 1998, Ph.D. Thesis, École Polytechnique, Palaiseau, France
Hill, N. A., & Whaley, K. B. 1996a, J. Electronic. Mat., 25, 269
Hill, N. A., & Whaley, K. B. 1996b, Phys. Rev. Lett., 76, 3039
Hofmeister, H., Huisken, F., & Kohn, B. 1999, Eur. Phys. J. D, 9, 137
Huffman, D. R. 1977, Adv. Phys., 29, 129
Huisken, F., Hofmeister, H., Kohn, B., Laguna, M. A., & Paillard, V. 2000, Appl. Surf. Sci., 154, 305
Huisken, F., Kohn, B., Alexandrescu, R., et al. 1999a, J. Nanopart. Res., 1, 293
Huisken, F., Kohn, B., & Paillard, V. 1999b, Appl. Phys. Lett., 74, 3776
Inoue, Y., Tanaka, A., Fujii, M., Hayashi, S., & Yamammoto, K. 1999, J. Appl. Phys., 86, 3199
Kachurin, G., Zhuravlev, K. S., Pazdnikov, N. A., et al. 1997, Nucl. Instrum. Meth. B, 127, 583
Kerr, T. H., Hurst, M. E., Miles, J. R., & Sarre, P. J. 1999, MNRAS, 303, 446
Kubin, R. F., & Fletcher, A. N. 1982, J. Luminescence, 27, 455
Ledoux, G., Ehbrecht, M., Guillois, O., et al. 1998, A&A, 333, L39

Ledoux, G., Guillois, O., Porterat, D., et al. 2000a, Phys. Rev. B, 62, 15942
Ledoux, G., Guillois, O., Reynaud, C., et al. 2000b, Mater. Sci. Engin. B, 69, 350
Liedtke, S., Lips, K., Bort, M., Jahn, K., & Fuhs, W. 1989, J. Noncryst. Sol., 114, 522
Linnros, J., Lalic, N., & Grivickas, A. G. V., 1999, J. Appl. Phys., 86, 6128
Lonfat, M., Marsen, B., & Sattler, K. 1999, Chem. Phys. Lett., 313, 539
Meyer, B. K., Hofmann, D. M., Stadler, W., et al. 1993, Appl. Phys. Lett., 63, 2120
Murakami, K., Suzuki, T., Makimura, T., & Tamura, M. 1999, Appl. Phys. A, 69, S13
Papoular, R., Conrad, J., Guillois, O., et al. 1996, A&A, 315, 222
Perrin, J.-M., Darbon, S., & Sivan, J.-P., 1995, A&A, 304, L21
Perrin, J.-M., & Sivan, J.-P. 1992, A&A, 255, 271
Rouan, D., Lecoupanec, P., & Leger, A. 1995, in Proc. of 1st Franco-British meeting on the physics and chemistry of the interstellar medium, ed. C. S. Jeffery, 22, 37
Rush, W. F., & Witt, A. N. 1975, AJ, 80, 31
Sakata, A., Wada, S., Narisawa, T., et al. 1992, ApJL, 393, L83
Schmidt, G. D., Cohen, M., & Margon, B. 1980, ApJL, 239, L133
Shimizu-Iwayama, T., Kurumado, N., Hole, D. E., & Townsend, P. D. 1998, J. Appl. Phys., 83, 6018
Siebert, W., Carius, R., Fuhs, W., & Jahn, K. 1987, Phys. Stat. Sol. (b), 140, 311
Sivan, J.-P., & Perrin, J.-M. 1993, ApJ, 404, 528
Smith, T. L., Witt, A. N., & Gordon, K. D. 1999, A&AS Meeting, 194, 71.13
Terranova, M. L., Piccirillo, S., Sessa, V., Botti, S., & Rossi, M. 1999, Appl. Phys. Lett., 74, 3146
Tessler, L. R., & Solomon, I. 1995, Phys. Rev. B, 52, 10962
Theiss, W. 1997, Surf. Sci. Rep., 29, 91
Vasil'ev, V. A., Volkov, A. S., Musabekov, E., Terukov, E. I., & Chernyshov, S. V. 1990, Sov. Phys. Solid State, 32, 462
Vial, J.-C. 1999, private communication
Vial, J.-C., Herino, R., Billat, S., et al. 1992, IEEE trans. Nuc. Sci., 39, 563
Waters, L. B. F. M., Cami, J., de Jong, T., et al. 1998, Nature, 391, 868
Wdowiak, T. J., Donn, B., Nuth, J. A., Chappelle, E., & Moore, M. 1989, ApJ, 336, 838
Webster, A. 1993, Mon. Not. R. Astron. Soc., 264, L1
Wehrspohn, R. B., Chazalviel, J.-N., Ozanam, F., & Solomon, I. 1999, Eur. Phys. J. B, 8, 179
Witt, A., & Schild, R. 1985, ApJ, 294, 225
Witt, A., & Schild, R. 1988, ApJ, 325, 837
Witt, A., Schild, R., & Kraiman, J. 1984, ApJ, 281, 708
Witt, A. N. 1988, Proceedings of the Conference Dust in the Universe (Cambridge University, Press), 1
Witt, A. N. 1999, private communication
Witt, A. N., & Boroson, T. A. 1990, ApJ, 355, 182
Witt, A. N., Gordon, K. D., & Furton, D. G. 1998, ApJL, 501, L111
Witt, A. N., Ryutov, D., & Furton, D. G. 1996, in From Star Dust to Planetesimals, Santa Clara, NASA
Wolkin, M. V., Jorne, J., Fauchet, P. M., Allan, G., & Delerue, C. 1999, Phys. Rev. Lett., 82, 197
Xu, S., Hundhaussen, M., Ristein, J., Yan, B., & Ley, L. 1993, J. Noncryst. Sol., 164, 1127
Zubko, V., Smith, T., & Witt, A. 1999, ApJ, 511, L57